Nano Today 61 (2025) 102626

Contents lists available at ScienceDirect

Nano Today

journal homepage: www.elsevier.com/locate/nanotoday

Hafnium oxide-based sensitizer with radiation-triggered cuproptosis for radiotherapy

Xue Wang [a,b,1], Dongmei Wang [a,b,1], You Liao [a,b], Xihong Guo [a], Qingwei Song [b,c], Wenchao Liu [a,b], Chenglu Gu [a,b], Shuanglong Du [a,b], Baoyun Sun [a,b,*], Zhanjun Gu [a,b,*]

[a] CAS Key Laboratory for Biomedical Effects of Nanomaterials and Nanosafety, Institute of High Energy Physics, Chinese Academy of Sciences, Beijing 100049, China
[b] University of Chinese Academy of Sciences, Beijing 100049, China
[c] Laboratory of Advanced Theranostic Materials and Technology, Ningbo Institute of Materials Technology and Engineering, Chinese Academy of Sciences, Ningbo 315201, China

ARTICLE INFO

Keywords:
Cuproptosis
Hafnium oxide
Radiotherapy
Tumor
Radiosensitization

ABSTRACT

Advanced sensitizers hold significant clinical importance in improving precise tumor radiotherapy while minimizing harm to normal tissues. In our work, the HfO_2-based radiosensitizer (ES@HM-HfO_2:Cu) is developed, in which Cu ions are doped in the shell of the HfO_2 nanocapsules, and elesclomol (ES), the Cu ionophore, is filled in the hollow mesoporous structure. Following the X-ray irradiation, ES@HM-HfO_2:Cu nanocapsules with high-energy deposition effect enable precise and controllable release of Cu ions within the tumor to trigger cuproptosis, exerting dual sensitization outcomes. Consequently, the ES@HM-HfO_2:Cu, leveraging the advantage of cuproptosis activation, achieves a tumor inhibition rate of 77.9 % with no apparent toxicity. Notably, the cuproptosis induced by the released Cu ions from ES@HM-HfO_2:Cu nanocapsules under X-ray irradiation reinforces the sensitization of HM-HfO_2 by promoting mitochondrial lipoylated protein aggregation and iron-sulfur cluster protein loss. Hence, the innovative HfO_2-based radioenhancer achieves intensified radiosensitization through X-ray-responsive cuproptosis, offering profound medical implications for advancing clinical radiotherapy.

Introduction

Radiotherapy is a potent therapeutic modality for malignant tumors, yet the persistent challenge lies in the "dose-limiting toxicity" hindering therapeutic efficacy [1]. To achieve precise tumor radiotherapy while minimizing damage to healthy tissues, developing advanced sensitizers is a critical strategy [2]. Inorganic nanoparticles incorporating high-Z elements, such as hafnium dioxide (HfO_2), Gd chelates, and gold, can augment radiation dose deposition within local tumors and increase the variety and amount of reactive oxygen species through physical mechanisms [3–5]. Among these, HfO_2 serves as the primary component in NBTXR3 (Nanobiotix), an FDA-approved physical radioenhancer, known for its exceptional ionizing radiation (IR) absorption efficiency and satisfactory safety profile [1]. In a series of clinical evaluation trials, NBTXR3 has substantially augmented tumor suppression in the management of various malignancies, including lung cancer, pancreatic cancer, head and neck cancer, soft tissue sarcoma, and others, especially in conjunction with chemotherapy or immunotherapy agents [6–11]. It is important to highlight that HfO_2 features facile metal ions doping and adjustable structures [12–14]. These are untapped innate advantages for further exploring the potential multiple sensitization mechanisms of HfO_2 to improve tumor radiosensitivity and pioneer clinical progress.

Abbreviations: HfO_2, hafnium dioxide; RT, radiotherapy; IR, ionizing radiation; ES, elesclomol; TCA, tricarboxylic acid; Fe-S, iron-sulfur; FDX1, ferredoxin 1; DLAT, dihydrolipoamide S-acetyltransferase; XPS, X-ray photoelectron spectroscopy; XAFS, X-ray absorption fine structure; SER_{10}, ensitization enhancement ratio; ES-Cu, elesclomol-$CuCl_2$; Bio-TEM, biological electron microscopy; POLD1, polymerase DNA delta 1 catalytic subunit; ACO2, Aconitase 2; LIAS, lipoyl synthase; HSP70, heat shock protein 70; H&E, hematoxylin and eosin; TUNEL, terminal deoxynucleotidyl transferase-mediated dUTP nick-end labeling; SR-μXRF, synchrotron radiation micro-X-ray fluorescence; LA, lipoic acid; PBS, phosphate-buffered saline.

* Corresponding authors at: CAS Key Laboratory for Biomedical Effects of Nanomaterials and Nanosafety, Institute of High Energy Physics, Chinese Academy of Sciences, Beijing 100049, China.
E-mail addresses: sunby@ihep.ac.cn (B. Sun), zjgu@ihep.ac.cn (Z. Gu).
[1] Xue Wang and Dongmei Wang contributed equally to this work.

https://doi.org/10.1016/j.nantod.2024.102626
Received 29 September 2024; Received in revised form 2 December 2024; Accepted 26 December 2024
Available online 31 December 2024

Based on these findings, next-generation HfO_2-based radiosensitizers integrating multiple sensitization functionalities have the potential to advance the development of radiosensitizers for clinical applications.

Tumor radiosensitivity enhancement based on nanomaterials containing manganese, iron, and other transition metals is an attractive alternative by interacting with the tumor microenvironment, disrupting metabolism, inducing ferroptosis, or stimulating immune responses [15–22]. Recently, a novel cell death mode (cuproptosis) induced by the excessive accumulation of intracellular Cu ions has garnered significant attention, particularly in terms of tumorigenesis and cancer therapy associated with dysregulated copper metabolism [23,24]. Cuproptosis relies on copper ionophores, exemplified by elesclomol (ES), to accumulate Cu ions continuously through chelating extracellular Cu^{2+} and selectively target mitochondria [25]. Cu ions directly bind to lipoylated components of the tricarboxylic acid (TCA) cycle, resulting in lipoylated protein aggregation and the iron-sulfur (Fe-S) cluster protein loss, which induces proteotoxic stress and eventually cell death [26]. Studies have identified the potential of cuproptosis to enhance tumor radio-immunotherapy and improve radiosensitivity of radioresistant tumors, portending the development of advanced radiosensitizers with cuproptosis-inducing function represents a promising strategy for improving the efficacy of tumor therapy [26–29]. However, an excess of Cu ions can result in systemic toxicity [30]. Therefore, strategically utilizing the localized radiation property of radiotherapy to increase Cu ion concentration within tumor cells emerges as a critical issue that warrants thoughtful consideration [30].

Inspired by this, we propose an innovative HfO_2-based radiosensitizer with cuproptosis-triggered functionality to exert tumor suppression for radiotherapy. In our scheme, the Cu-doped HfO_2 nanocapsules with a hollow mesoporous structure are synthesized using a straightforward doping method, enabling controlled release and transformation of Cu ions at the tumor site in response to X-ray irradiation. On the one hand, irradiation-released Cu ions are delivered to tumor cells by the copper ionophores ES loaded in the mesoporous shell and hollow cavity structure of the nanocages, where they interact with ferredoxin 1 (FDX1) and protein lipoylation. On the other hand, part of the Cu^{2+} ions are reduced to the more toxic Cu^{+} ions during irradiation. These Cu ions will affect the Fe-S cluster proteins of the mitochondrial respiratory chain complex and promote the aggregation of dihydrolipoamide S-acetyltransferase (DLAT). Notably, the ES@HM-HfO_2:Cu without obvious biological toxicity showcases enhanced radiosensitization and inhibitory efficacy on tumor cell proliferation in contrast to the physical sensitizer HfO_2. Overall, the cuproptosis-activated HfO_2-based radiosensitizer based on X-ray stimulation indicates promising potential for clinical application and provides a new paradigm for optimizing the clinical sensitization efficacy of HfO_2.

Experimental section

Preparation of ES@HM-HfO_2:Cu nanocapsules

The monodispersed SiO_2 sacrificial templates were prepared using the Stöber method. Subsequently, the SiO_2 spheres were dispersed in a mixed solution of ethanol and acetonitrile at a volume ratio of 3:1, with the addition of ammonia solution, followed by thorough mixing and stirring. The solution containing $C_{16}H_{36}HfO_4$ (70 % in n-butanol) and Cu $(NO_3)_2{\cdot}H_2O$ in ethanol (a molar ratio of Hf to Cu of 6:1) was introduced and allowed to react for 6 h at room temperature. The resulting SiO_2@HfO_2:Cu intermediate underwent centrifugation and subsequent washing. The SiO_2 template was removed by etching with a 10 M sodium hydroxide solution, yielding HM-HfO_2:Cu nanocages. Finally, HM-HfO_2:Cu nanocages were sufficiently mixed with ES (copper ionophore) for enough time to obtain ES@HM-HfO_2:Cu nanocapsules.

Radiation-induced release of Cu^{+} from HM-HfO_2:Cu

The neocuproine reagent and hydroxylamine hydrochloride were added sequentially to $CuCl_2$ solutions with varying concentrations. After thorough mixing and a 5-min reaction period, the absorbance was measured at 457 nm to create a standard curve correlating Cu^{+} concentration with absorbance readings. Cu^{+} in a 2 mg mL^{-1} HM-HfO_2:Cu aqueous solution following exposure to varying radiation doses (0–30 Gy) was analyzed using the neocuproine reagent-based method. To explore the reduction mechanism of Cu^{+} ions in HM-HfO_2:Cu post-irradiation, either the electron quencher KNO_3 or the hydroxyl radical (•OH) quencher NaAc at a concentration of 2 mM was added to a solution containing 2 mg mL^{-1} HM-HfO_2:Cu and 3 mM neocuproine. Subsequently, the solution was irradiated at 30 Gy, and its absorbance was monitored to determine the concentration of Cu^{+}.

Specific detection of intracellular Cu^{+}

The Coppersensor-1 specific probe was employed to detect the Cu^{+} levels within 4T1 cells. 4T1 cells (1×10^5 per well) were cultured in confocal laser scanning microscopy (CLSM) dishes with complete media containing 10% fetal bovine serum (CTCC-002-071). After cell attachment, phosphate-buffered saline (PBS), HM-HfO_2:Cu, ES, or ES@HM-HfO_2:Cu were added to the dishes and incubated for 8 h. Following this, Coppersensor-1 (at a final concentration of 5 μM) was introduced to the dishes before X-ray irradiation (4 Gy). Subsequent cellular imaging was performed using CLSM.

DLAT immunofluorescence assay

4T1 cells (2×10^5 per well) were seeded onto cell slides. Upon adherence, the cells were treated with PBS, HM-HfO_2:Cu, ES, or ES@HM-HfO_2:Cu for 8 h before exposure to X-ray irradiation (0 or 4 Gy). Mitochondria were pre-stained with MitoTracker to facilitate the observation of DLAT aggregation. Specific primary antibodies were applied to target the proteins in the cells using conventional immunofluorescence staining techniques. A fluorescently labeled secondary antibody was subsequently used to visualize DLAT as green fluorescence under confocal microscopy. Finally, the specimens were examined using CLSM.

In vivo tumor radiotherapy models and antitumor efficacy assay

Female BALB/c mice (6 weeks old, sourced from Beijing PSF Bioscience Co., Ltd.) were injected with 50 μL of a PBS suspension containing 5×10^5 4T1 cells into the subcutaneous tissue of the right abdomen[31]. When the average tumor volume reached 100 mm^3, all mice were randomly allocated into six groups (n = 8, representing biologically independent experiments): PBS, ES@HM-HfO_2:Cu, IR, HM-HfO_2:Cu + IR, ES + IR, and ES@HM-HfO_2:Cu + IR. Subsequently, the mice received intratumoral administration of the drugs (50 μL, [HM-HfO_2:Cu]=20 mg mL^{-1}, [ES]=2 μM; ES@HM-HfO_2:Cu is a combination of the two drugs mentioned above). The treatment regimen involved drug injections administered 4 h before X-ray irradiation for three consecutive days. The body weight and tumor volume of all mice were monitored every other day for 20 days. Tumor volume (V) was calculated using the formula: $V = (\text{Length} \times \text{Width}^2) / 2$. The tumor growth inhibition ratio (TGI) was calculated as $TGI = 1 - V/V_{PBS}$, where V is the volume of the tumor at the end of treatment for different treated groups [32].

Correspondence analysis of elemental distribution and damage in tumor tissues

The spatial distribution of Cu and Hf elements within mice tumor tissues was analyzed with synchrotron radiation micro X-ray

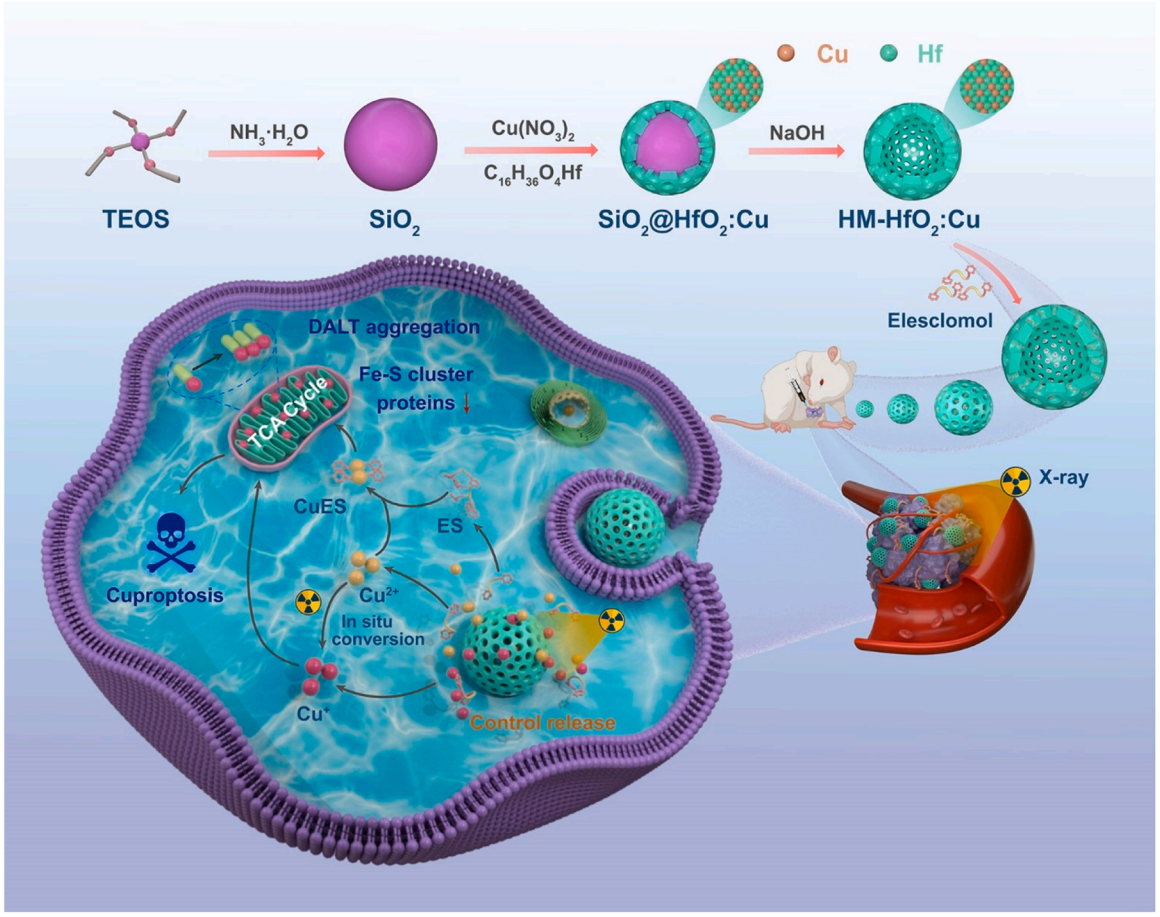

Scheme 1. Fabrication process and schematic illustration of ES@HM-HfO_2:Cu for oncotherapy. Created using Cinema 4D and Adobe Illustrator. As X-ray responsive cuproptosis-activator HfO_2-based nanocapsules, ES@HM-HfO_2:Cu initiated the controlled release and in situ reduction of Cu ions upon exposure to X-rays. Irradiation-released Cu ions were delivered to the mitochondria by the Cu ionophores ES encapsulated within the nanocages, where they interacted with Fe-S cluster proteins and transformed into the more toxic Cu^+. Additionally, co-action with Cu^+ ions produced by irradiation reduction promoted DLAT aggregation. Finally, the proteotoxic stress generated by excess Cu ions triggered cuproptosis, thereby enhancing the radioenhancement effect of HfO_2 and resulting in efficient tumor radiosensitization.

fluorescence (SR-μXRF) technology. Specifically, intratumoral injections of ES@HM-HfO_2:Cu (20 μL, [HM-HfO_2:Cu] = 50 mg mL^{-1}, [ES] = 5 μM) were administered once the tumor volume reached 70 mm^3. After 4 h, the tumors underwent X-ray irradiation (6 Gy). Tumor samples collected at various time points were frozen at -80 °C and processed into frozen sections (40 μm thick) from the largest cross-section for subsequent 2D elemental mapping acquisition at the 4W1B beamline of Beijing Synchrotron Radiation Facility. To minimize errors, tissue sections for H&E and TUNEL analysis were obtained immediately adjacent to the two layers mentioned earlier.

Histological study

In assessing the therapeutic mechanisms in animal models, tumors were collected on the second day following three consecutive days of treatment. Subsequent analyses, including H&E staining, TUNEL staining, and immunofluorescence assessments for FDX1, LIAS, HSP70, DLAT, and LA, were conducted. All collected tumors were fixed in 4 % paraformaldehyde, and processed for embedding, sectioning, and staining. Statistical analysis was then performed on the relevant parameters in the stained tumor tissue sections.

Data analysis

The statistical data were presented as mean values ± standard deviation (SD). Statistical significance among multiple groups was assessed using ordinary one-way analysis of variance (ANOVA). Pairwise comparisons between specific groups were conducted using a two-tailed Student's *t*-test. The analysis was performed using GraphPad Prism (8.0.2). Statistical significance was defined as a P value of less than 0.05 [33].

Results and discussion

Preparation and Characterization of HM-HfO_2:Cu nanocages

On-demand release of Cu ions at tumor sites, while minimizing the impact on healthy tissues, is crucial for strengthening the radiosensitization outcomes of cuproptosis[34]. Thus, HM-HfO_2:Cu nanocages were developed, enabling the local, controllable release of Cu ions at tumor sites in response to X-ray stimulation. The construction of HM-HfO_2:Cu nanocages (Scheme 1) involved the synthesis of SiO_2 sacrificial templates (Figure S1), the assembly of SiO_2@HfO_2:Cu core-shell structures (Figure S2), and subsequently the alkali etching reaction to obtain the HM-HfO_2:Cu nanocages (Figures S3a-**c and** Table S1), in which the Cu ions were introduced into the HfO_2 shell structure through a straightforward one-step co-condensation procedure [35]. The HM-HfO_2:Cu nanocages had a hollow spherical structure with a diameter of approximately 100 ± 5 nm and a shell thickness of approximately 10 nm (Fig. 1**a and b**). The surface area and average pore

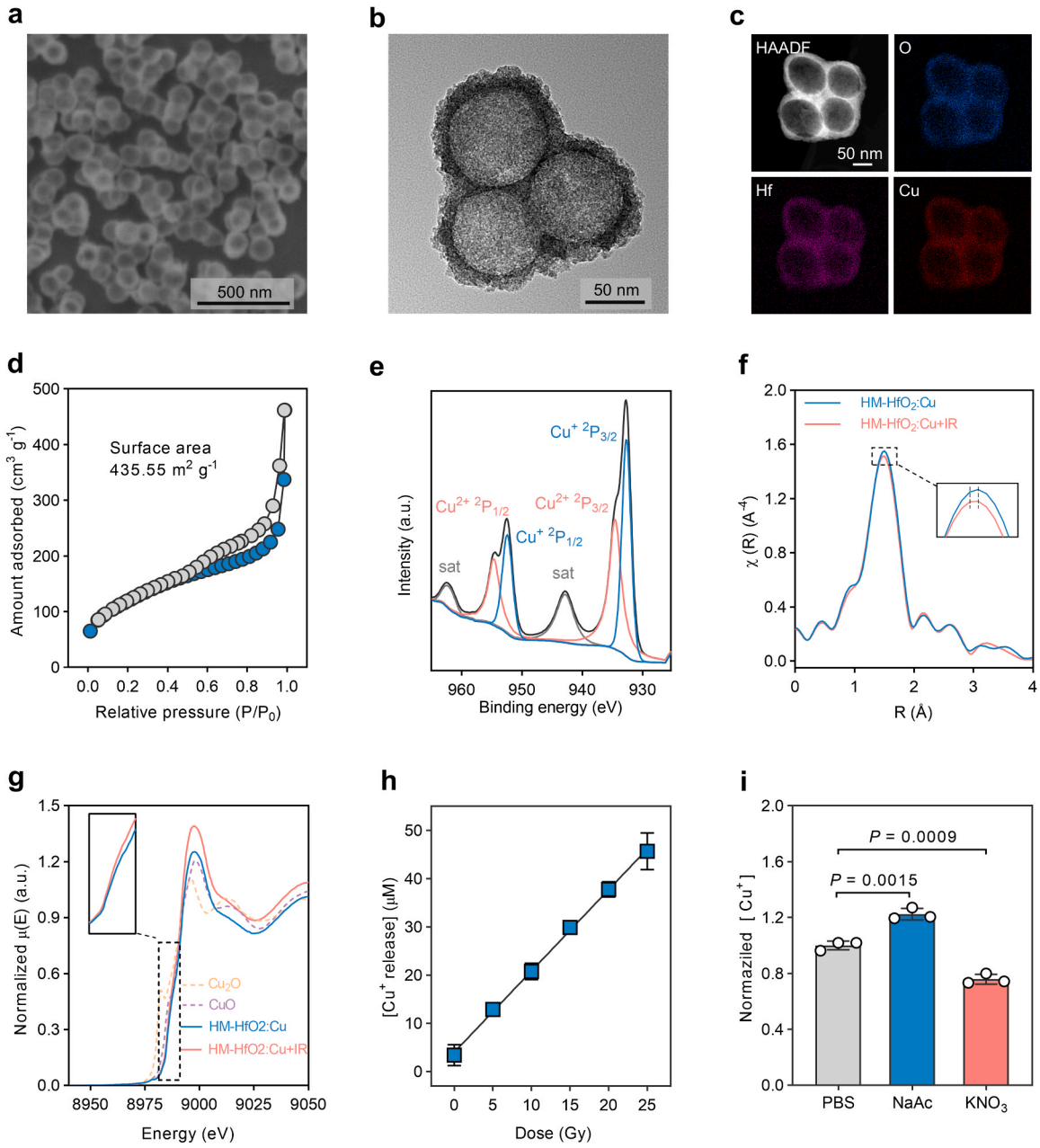

Fig. 1. Structural and performance characterizations of HM-HfO_2:Cu nanocages. a, SEM image, and b, TEM image of HM-HfO_2:Cu. c, High-angle annular dark field image and corresponding elemental mappings of HM-HfO_2:Cu. d, N_2 adsorption-desorption isotherm of HM-HfO_2:Cu. e, High-resolution XPS spectrum of Cu 2p in HM-HfO_2:Cu. f, The corresponding Cu k^2-weighted Fourier transform of HM-HfO_2:Cu and IR-irradiated HM-HfO_2:Cu. g, Cu K-edge XANES profiles of Cu_2O, CuO, HM-HfO_2:Cu and IR-irradiated HM-HfO_2:Cu. h, X-ray triggered Cu^+ ions release from HM-HfO_2:Cu nanocages detected with specific agent neocuproine, n = 3. i, Normalized concentration of Cu^+ ions released from HM-HfO_2:Cu nanocages treated with NaAc (•OH quencher) or KNO_3 (e^-_{aq} quencher) after X-ray exposure, n = 3. Data were represented as mean ± SD in h and i. Statistical analysis was performed using a two-tailed paired Student's *t*-test in i.

size of the HM-HfO_2:Cu nanocages were determined to be 435.55 $m^2\ g^{-1}$ and 7.83 nm, through N_2 adsorption-desorption isotherms (Fig. 1**d and** Figure S3d). Moreover, the Cu in HM-HfO_2:Cu was evenly dispersed within the HfO_2 shell structure and existed in the form of Cu-O bonds (Fig. 1**c and e**). The X-ray photoelectron spectroscopy (XPS) analysis revealed the presence of two Cu^{2+} satellite peaks, a distinct Cu^+ $2p_{3/2}$ peak and a stronger Cu^+ $2p_{1/2}$ peak, in addition to the Cu^{2+} $2p_{3/2}$ peak and Cu^{2+} $2p_{1/2}$ peak. Additionally, the HM-HfO_2:Cu nanocages, which display excellent dispersibility in various solutions and structure stability under irradiation (Figures S4 and S5), demonstrate promising biocompatibility and potential for in vivo applications.

Further, the properties of Cu in HM-HfO_2:Cu nanocages after exposure to X-rays were investigated utilizing the synchrotron X-ray absorption fine structure (XAFS) technique. Notably, the Cu-O bond in HM-HfO_2:Cu contracted slightly after irradiation (Fig. 1**f and** Table S2), implying that high-energy X-ray induces changes in the coordination environment of HM-HfO_2:Cu [36]. Meanwhile, the change in the valence of Cu within the nanocages was observed following X-ray exposure, where the absorption edge of the irradiated material skewed to a more reduced Cu^+ state compared to the unirradiated material (Fig. 1**g**). This alteration in valence could stem from the interaction between Cu^{2+} and high energy X-rays themselves or reductive products of irradiated ionized water [37,38]. Next, the specialized reagent neocuproine (a specific reagent for Cu^+ detection) was performed to monitor the release of Cu^+ ions from nanocages after X-ray irradiation. The amount of Cu^+ liberated from the HM-HfO_2:Cu post-X-ray

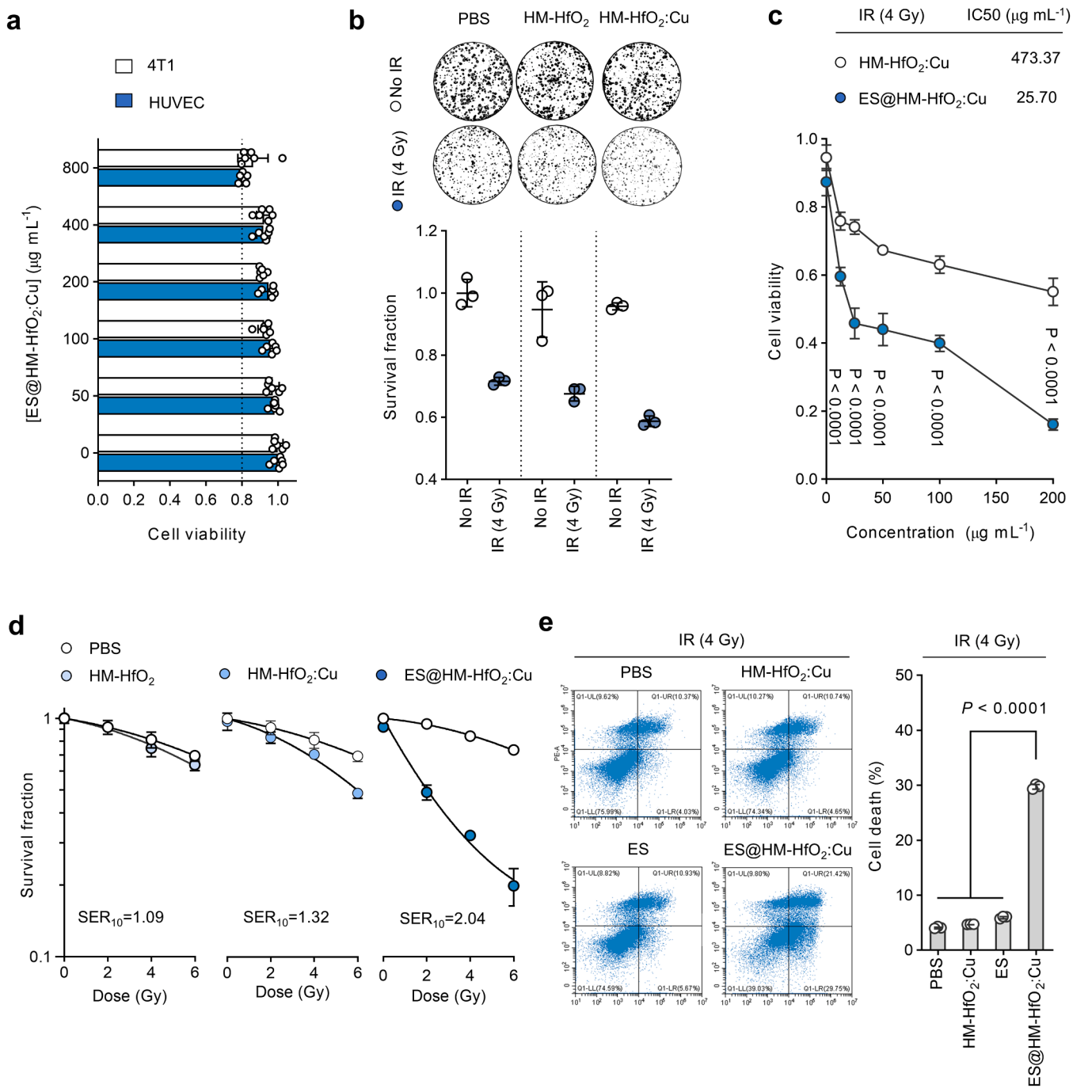

Fig. 2. In vitro radiosensitization outcomes with HM-HfO_2:Cu nanocages and ES@HM-HfO_2:Cu nanocapsules. a, Cytotoxicity of HM-HfO_2:Cu nanocages for 4T1 cells and HUVEC cells, n = 6. b, Colony formation analysis and images of 4T1 cells treated with different treatments, n = 3. c, Cytotoxicity of HM-HfO_2:Cu or ES@HM-HfO_2:Cu under X-ray irradiation on 4T1 cells, n = 6. d, Survival fraction of HM-HfO_2, HM-HfO_2:Cu, and ES@HM-HfO_2:Cu, n = 3. e, Cell death analysis, n = 3. All data were representative of independent experiments and were expressed as mean ± SD. Statistical analysis was performed using a two-tailed paired Student's *t*-test in c and d.

irradiation exhibited a direct and positive correlation with irradiation dosage (Fig. 1**h**), indicating that irradiation could promote the reduction and controllable release of Cu. Moreover, considering the possible impact of strongly reducing reactive hydrated electrons (e^-_{aq}, E^0 = 2.89 V) produced by irradiation ionization hydrolysis on the radiation-induced conversion of Cu^{2+} to Cu^+ (E^0 (Cu^{2+}/Cu^+) = 0.16 V vs NHE), the NaAc (sodium acetate, the quenching agent of •OH) and KNO_3(the quenching agent of e^-_{aq}) were used to explore the mechanism of Cu reduction by reductive products [39]. The concentration of Cu^+ ions in the NaAc-added group was higher compared to the control group, whereas the KNO_3-treated group showed the opposite trend (Fig. 1**i**). This was attributed to the role of NaAc in reducing the oxidative irradiation product •OH, thereby relatively facilitating the generation of additional e^-_{aq} and consequently enhancing the production of Cu^+ [40]. In conclusion, the HM-HfO_2:Cu nanocages with high specific surface area and mesoporous structure could release and produce abundant toxic Cu^+ ions in a controlled manner under X-ray irradiation, laying the foundation for precise and efficient induction of cuproptosis-sensitizing radiotherapy at the tumor site.

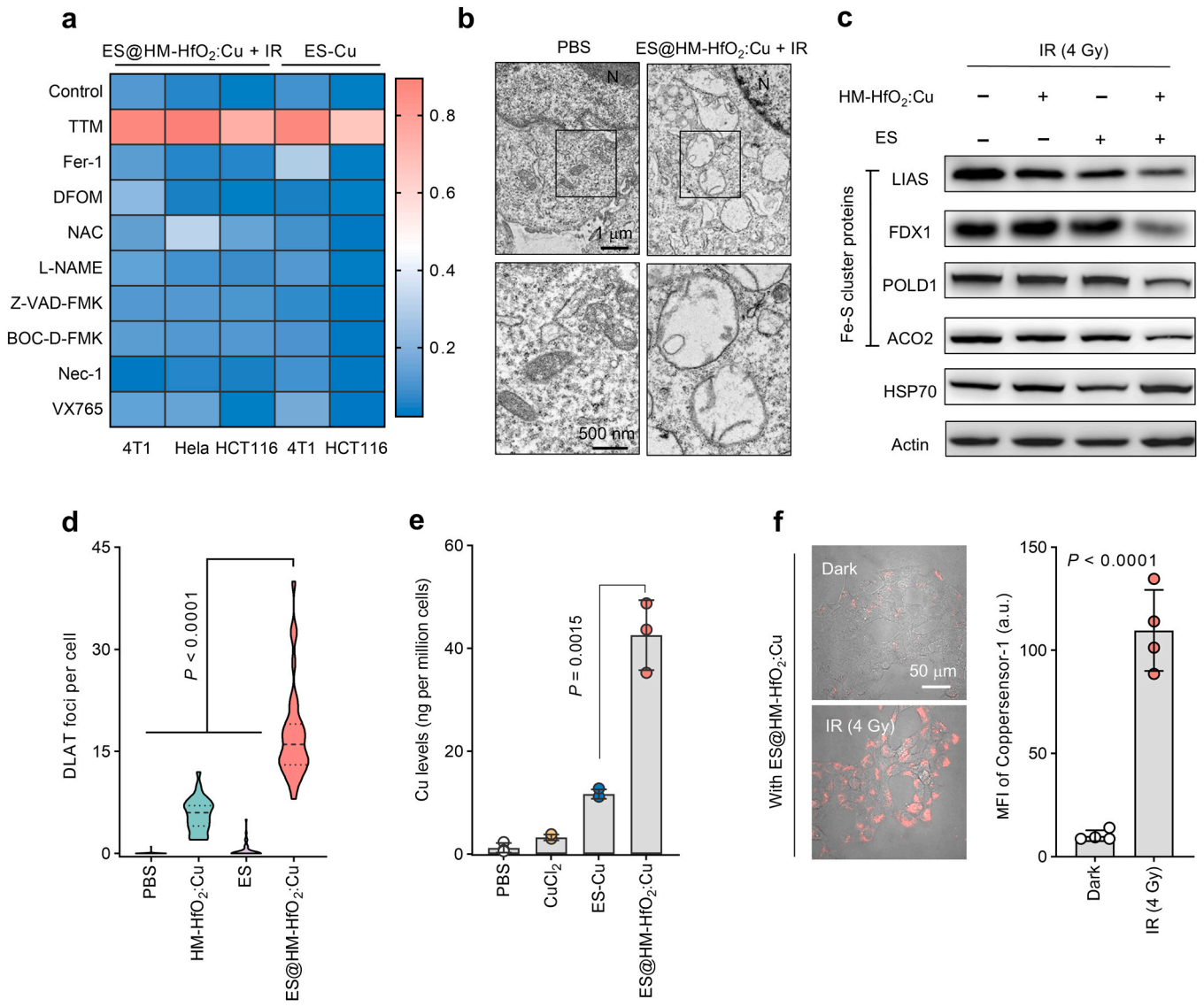

Fig. 3. Nature of cell death induced by ES@HM-HfO2:Cu combined with IR (4 Gy). a, Heatmap of cell viability incubated with diverse cell death inhibitors and treated with ES@HM-HfO_2:Cu combined IR, 30 nM elesclomol-$CuCl_2$ (1:1, ES-Cu) for 60 h, cell death inhibitors including ferroptosis inhibitor (ferrostatin-1, Fer-1), iron chelator (DFOM), oxidative stress inhibitor (N-acetylcysteine, NAC), NOS inhibitor (L-NAME), apoptosis inhibitors (Z-VAD-FMK and BOC-D-FMK), necrosis inhibitor (necrostatin-1, Nec-1), and pyroptosis inhibitor (VX765), n = 6. b, Representative Bio-TEM images of 4T1 cells treated with or without ES@HM-HfO_2:Cu combined with IR. c, Western blot of cuproptosis-associated proteins in different conditions. d, Counts of DLAT foci per 4T1 cell treated under various conditions and IR, n = 30. e, Cu levels assessed in cells following different conditions. f, Representative confocal images of Cu^+ in 4T1 cells and corresponding fluorescence intensity (arbitrary units, a.u.), n = 4. Data were expressed as mean ± SD. Statistical analysis was performed using a two-tailed paired Student's *t*-test in e-f and ordinary one-way ANOVA in d.

In vitro therapeutic effect of HM-HfO_2:Cu nanocages and ES@HM-HfO_2:Cu nanocapsules

Drawing upon the potential of controlled release of Cu ions in response to X-rays, the radiotherapy effects of HM-HfO_2:Cu nanocages were evaluated at the cellular level. Compared to biocompatible HM-HfO_2 (Figure S6a), HM-HfO_2:Cu with favorable cellular safety (Fig. 2**a and** Figure S6b) and the effectively internalized (Figure S7) demonstrated additional radiotherapy inhibitory effects against 4T1 tumor cells (Fig. 2**b**). In the clonogenic survival assay, the sensitization enhancement ratio (SER_{10}) of HM-HfO_2:Cu increased to 1.32, compared to 1.09 of HM-HfO_2 (Fig. 2**d and** Figure S8), which could be attributed to the release of Cu from HM-HfO_2:Cu under irradiation. To make the utmost of released Cu ions in efficiently triggering cuproptosis for more efficient radiotherapy sensitization, the HM-HfO_2:Cu with the 10 nM copper ionophores (ES) without obvious toxicity were co-mixed for enough time to create ES@HM-HfO_2:Cu nanocapsules (Figure S9). After 4 Gy irradiation, the tumor cell-killing effect of ES@HM-HfO_2:Cu nanocapsules was significantly enhanced compared to the HM-HfO_2:Cu at the same concentration (Fig. 2**c**). Moreover, the ES@HM-HfO_2:Cu + IR treatment group exhibited a conspicuous inhibitory effect on 4T1 cell proliferation, with SER_{10} reaching as high as 2.04 (Fig. 2**d and** Figure S10), highlighting the potential of ES@HM-HfO_2:Cu for enhancing radiotherapy sensitivity. Furthermore, cell death assessment validated the substantial radiosensitizing effect of ES@HM-HfO_2:Cu and IR, with a cell death rate 7.3 times higher than that observed in the IR-only treated group (4.06–29.72 %) (Fig. 2**e and** Figure S11). Additionally, DNA damage was notably increased in cells treated with ES@HM-HfO_2:Cu and IR, being 3.8-fold higher compared to IR alone (Figure S12). These results regarding DNA damage and cell death levels validated that ES@HM-HfO_2:Cu nanocapsules had excellent sensitization properties for radiotherapy, which might result from the assisting

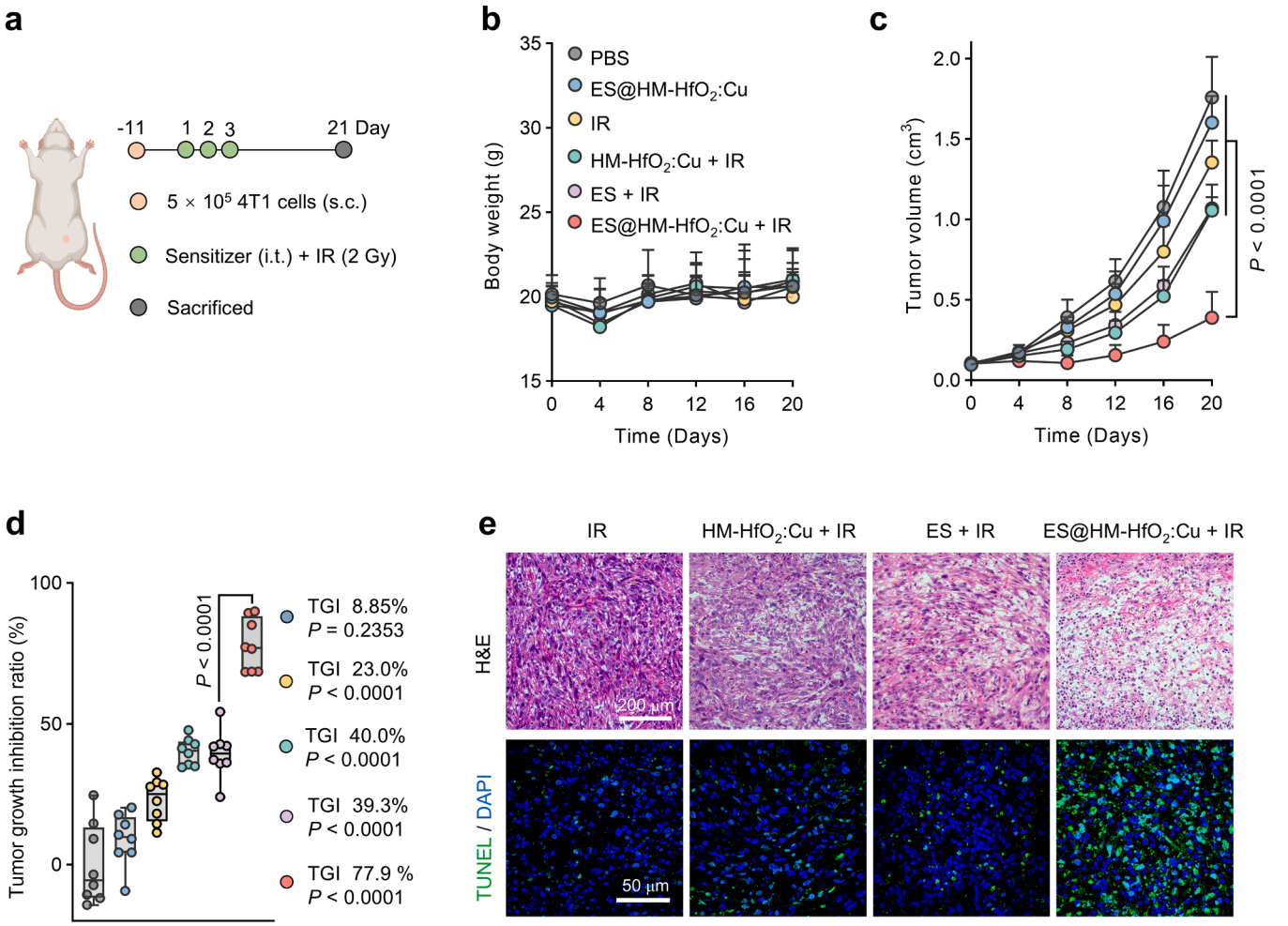

Fig. 4. In vivo radiosensitization therapy with ES@HM-HfO_2:Cu combined with IR. a, Treatment evaluation process. b, The body weight and c, the growth kinetics of 4T1 tumor-bearing mice. d, Tumor growth inhibition ratio. e, Expression of H&E and TUNEL staining in tumor sections following IR irradiation. Data in b, c, and d were represented as mean ± SD. Statistical analyses were performed using ordinary one-way ANOVA in c and d.

role of Cu ionophores ES on Cu ions released from nanocapsules.

In vitro therapeutic mechanism of ES@HM-HfO_2:Cu nanocapsules

Building upon the aforementioned radiosensitization outcomes of ES@HM-HfO_2:Cu nanocapsules, the investigations of radiosensitization mechanisms were further conducted. Various inhibitors of cell death pathways were employed in cell death rescue experiments, including ferroptosis inhibitors, oxidative stress inhibitors, apoptosis inhibitors, necrosis inhibitors, and pyroptosis inhibitors (Fig. 3**a**). Of interest, the cell survival rate of ES@HM-HfO_2:Cu nanocapsules and IR treatment group was significantly increased only when co-treated with the copper chelator sodium tetrathiomolybdate (TTM), consistent with the cuproptosis-positive control group (ES-Cu). Additionally, TTM also restored colony formation in 4T1 cells following ES@HM-HfO_2:Cu and IR treatment (Figure S13). The dominant form of cell death triggered by ES@HM-HfO_2:Cu and IR treatment was associated with cuproptosis, distinct from ferroptosis, apoptosis, pyroptosis, or necrosis. Considering the impact of cuproptosis on the TCA cycle in mitochondrial respiration, detailed validation of the alterations in related organelles and protein molecules is essential. First, notable swelling and complete morphological disruption were observed in the mitochondria of 4T1 cells treated with ES@HM-HfO_2:Cu and IR using the biological transmission electron microscope (Bio-TEM), contrasting with the normal mitochondria observed in the PBS-treated group (Fig. 3**b and** Figure S14). Simultaneously, a profound decrease in mitochondrial membrane potential of ES@HM-HfO_2:Cu and IR treatment group was also the evidence of mitochondrial dysfunction and damage (Figure S15). In addition, the expression level of Fe-S cluster proteins served as a crucial indicator of the occurrence of cuproptosis. Western Blot experiments demonstrated a significant decrease in Fe-S proteins, such as FDX1, POLD1, ACO2, and lipoyl synthase (LIAS) in 4T1 cells co-treated with ES@HM-HfO_2:Cu and IR (Fig. 3**c**). The expression of heat shock protein 70 (HSP70, a danger-associated molecular pattern) was also markedly increased. Additionally, aggregation of lipoylated protein DLAT was evident in the group of ES@HM-HfO_2:Cu and IR (Fig. 3**d and** Figure S16). These findings indicated that ES@HM-HfO_2:Cu nanocapsules combined with radiotherapy triggered proteotoxic stress linked to cuproptosis, consistent with the cuproptosis-positive control group (ES-Cu)[26].

The critical trigger for cuproptosis is the accumulation of excess Cu ions in cells. At the equivalent Cu ion concentration, cells treated with ES@HM-HfO_2:Cu took up more Cu than those treated with $CuCl_2$ and the cuproptosis-positive control group (ES-Cu)(Fig. 3**e**). Moreover, intracellular Cu^+ levels were assessed using the coppersensor-1 probe, showing a tenfold increase in Cu^+ content following ES@HM-HfO_2:Cu and IR treatment compared to ES@HM-HfO_2:Cu treatment alone (Fig. 3**f and** Figure S17). The Cu^+ signals in the unirradiated groups might come from intracellular reducing substances such as glutathione. The increased intracellular accumulation of the more toxic Cu^+ after X-ray exposure suggested that irradiation acted as the key trigger for the controlled release and reduction of Cu from ES@HM-HfO_2:Cu with inimitable mesoporous structure, leading to cuproptosis. In conclusion,

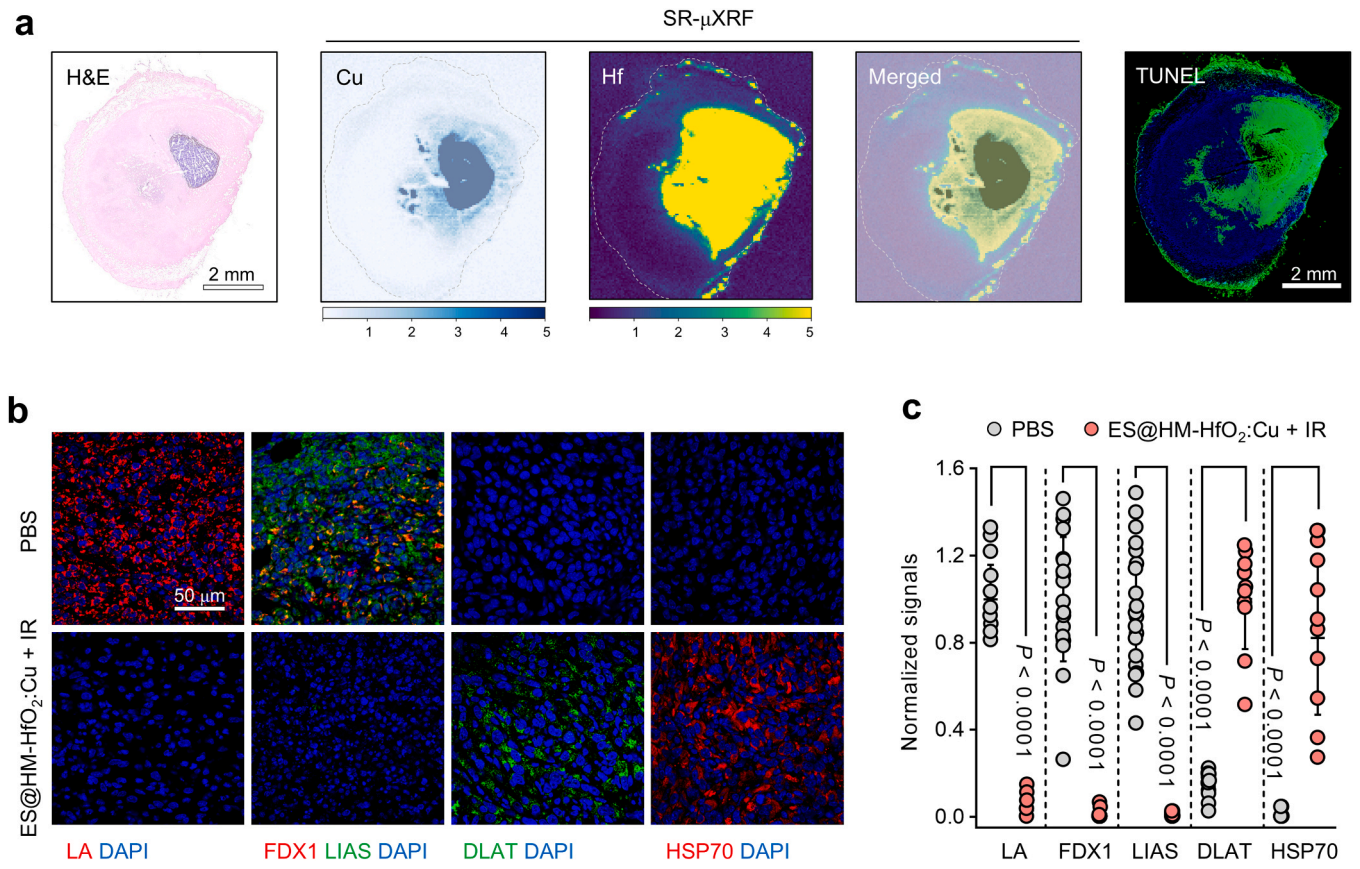

Fig. 5. In vivo radiosensitization mechanism of ES@HM-HfO_2:Cu combined with IR. a, SR-μXRF images of Cu and Hf elements in tumor tissue of mice treated with ES@HM-HfO_2:Cu combined with IR (X-ray, 6 Gy) after 72 h, and H&E and TUNEL staining of adjacent sections. b, Expression levels of LA, FDX1, LIAS, DLAT, and HSP70 and c, corresponding analysis within tumor sections treated with ES@HM-HfO_2:Cu combined with IR (X-ray, 2 Gy × 3), n ≥ 10. Data were represented as mean ± SD. Statistical analysis was performed using a two-tailed paired Student's *t*-test in c.

the radiosensitization outcomes resulting from the combination of ES@HM-HfO_2:Cu nanocapsules and radiotherapy were primarily attributed to cuproptosis, initiated by the accumulation of excess copper ions within 4T1 cells, in addition to the radiative energy deposition properties of HfO_2.

In vivo therapeutic effect of ES@HM-HfO_2:Cu nanocapsules

Motivated by the cellular results, an evaluation was conducted on the efficacy of cuproptosis-activator ES@HM-HfO_2:Cu nanocapsules for tumor therapy in animal models. Before therapeutic experiments, the reasonable safety profile of ES@HM-HfO_2:Cu in both pre- and post-irradiation was confirmed through hemolysis experiments (Figure S18). Next, we assessed the therapeutic efficacy using mice bearing 4T1 tumors as the experimental model, with a treatment protocol comprising intratumoral drug injection administered 4 h before X-ray irradiation for three consecutive days (Fig. 4**a**). The outcomes revealed a slowdown in tumor growth across all groups post-radiotherapy. Notably, tumor growth was markedly suppressed in the group receiving combined ES@HM-HfO_2:Cu and IR treatment, achieving the tumor growth inhibition (TGI) of 77.9 %, while effects observed in the ES@HM-HfO_2:Cu or IR group alone was less significant (Fig. 4**c-d and** Figures S19-S20). The aforementioned suppression disparity suggested that irradiation was crucial for the effective activation of ES@HM-HfO_2:Cu nanocapsules for tumor inhibition, stemming not only from the irradiation dose deposition property of HfO_2 but also from the release of more Cu ions upon irradiation. Further, tumor sections underwent H&E staining and TUNEL analysis, unveiling notable nucleolysis and cytoplasmic degradation in the tumor tissues of combined treatment of ES@HM-HfO_2:Cu and radiotherapy, alongside an increased presence of TUNEL-positive cells and a substantial decrease in tumor cell count (Fig. 4**e and** Figure S21). However, the above histological analysis was not distinctly observed in the ES@HM-HfO_2:Cu or IR-treated groups. These findings displayed that the cuproptosis-activator ES@HM-HfO_2:Cu nanocapsules exhibited a higher level of radiosensitization and an efficient tumor inhibition effect only under irradiation response.

In vivo therapeutic mechanism of ES@HM-HfO_2:Cu nanocapsules

Further analysis revealed the radiosensitization mechanism of ES@HM-HfO_2:Cu nanocapsules as a rulable cuproptosis-activator at the animal level. Initially, a correlation between the distribution of Cu within the tumor tissues and the sites of tumor injury was determined utilizing synchrotron radiation micro-X-ray fluorescence (SR-μXRF) technology (Fig. 5**a**). Furthermore, ES@HM-HfO_2:Cu nanocapsules persisted within the tumor for at least 72 h post-X-ray exposure (Figure S22), enabling continuous controlled release of Cu ions induced by IR. This sustained release mechanism could strengthen cuproptosis, potentially improving the effectiveness of fractionated radiosensitization.

Follow-up analysis unveiled the underlying mechanisms, highlighting the crucial role of X-ray-responsive ES@HM-HfO_2:Cu in triggering cuproptosis sensitization to radiotherapy. Immunofluorescence staining analysis elucidated a notable downregulation of lipoic acid (LA), LIAS and FDX1 expression, along with evident aggregation of DLAT proteins and the upregulation of HSP70 protein expression within the tumor tissues of the ES@HM-HfO_2:Cu + IR group (Fig. 5**b-c and**

Figures S23-S26). These findings aligned with sensitization mechanisms of cuproptosis triggered by excess Cu ions released by irradiation observed at the cellular level. Taken together, the decrease in Fe-S cluster proteins and aggregation of lipoylated proteins in tumors associated with cuproptosis elucidated the significant role of cuproptosis, efficiently induced by controlled release of Cu ions from radiotherapy-responsive ES@HM-HfO_2:Cu nanocapsules in antitumor effects.

Besides therapeutic effectiveness, the biosafety of nanomaterial is a crucial evaluation factor for its biological applications. The body weight of mice in all groups remained basically stable throughout the treatment period, indicating negligible in vivo toxicity or side effects associated with the ES@HM-HfO_2:Cu nanoparticles (Fig. 4**b**). No significant abnormalities were observed in the standard blood biochemistry, hematological parameters, or histological sections of normal organs in the groups at the end of the treatment cycle (Figures S27-S29). Collectively, intratumoral local injection of ES@HM-HfO_2:Cu nanocapsules not only demonstrated an acceptable safety profile but also maintained the efficient dose deposition effect of HfO_2 while facilitating the controlled release of Cu ions in response to X-rays at the tumor site, thus leading to precise induction of cuproptosis-sensitizing radiotherapy. Therefore, ES@HM-HfO_2:Cu nanocapsules, as a considerable HfO_2-based cuproptosis-activator, offer an effective strategy and alternative options for radiosensitization.

Conclusion

In conclusion, this work innovatively develops an X-ray-activated HfO_2-based radiosensitizer with cuproptosis-induced function, ES@HM-HfO_2:Cu. Under X-rays, Cu ions controllably release from ES@HM-HfO_2:Cu nanocapsules and partly reduce to Cu^+ at the tumor sites, which assists in the precise induction of cuproptosis for radiosensitization. These Cu ions will activate the FDX1-regulated protein-lipid acylation pathway of tumor cells, along with the downregulation of Fe-S cluster proteins due to FDX1 reducing Cu^{2+} (delivered to mitochondria by carrier ES) to more toxic Cu^+, the accumulation of DLAT proteins and the abundance of a danger-associated molecular pattern (HSP70), ultimately leading to acute proteotoxic stress and cuproptosis. In short, the strategy of ES@HM-HfO_2:Cu combination radiotherapy uniquely synergizes cuproptosis with radioenhancer HfO_2 to increase the radiosensitivity of cancer cells thereby significantly inhibiting tumor progression. Furthermore, the ES@HM-HfO_2:Cu nanocapsules have acceptable safety profiles, which provide a good foundation for the potential clinical application of nanocapsules.

Overall, our study enriches the sensitization characteristics of HfO_2-based nanomaterials by integrating cuproptosis with the radioenhancer HfO_2 in a unique approach. This innovative strategy serves as a valuable reference for radiosensitization drug development and offers a promising alternative to clinical radiosensitizers. Further research into this strategy is warranted to explore the value of HfO_2-based cuproptosis-activators in clinical radiotherapy.

CRediT authorship contribution statement

Baoyun Sun: Writing – review & editing, Supervision, Resources, Funding acquisition. **Wenchao Liu:** Investigation. **Qingwei Song:** Validation. **Shuanglong Du:** Investigation. **Chenglu Gu:** Investigation. **Dongmei Wang:** Writing – review & editing, Conceptualization. **Xue Wang:** Writing – original draft, Methodology, Investigation, Data curation, Conceptualization. **Xihong Guo:** Resources. **You Liao:** Conceptualization. **Zhanjun Gu:** Writing – review & editing, Supervision, Resources, Funding acquisition, Conceptualization.

Declaration of Competing Interest

The authors declare that they have no competing interests.

Acknowledgments

The authors acknowledge the National Key Research and Development Program of China (2022YFA1205900, 2020YFA0710702 and 2021YFA1201200), National Natural Science Foundation of China (22375205), Strategic Priority Research Program of Chinese Academy of Sciences (XDB36000000), Directional Institutionalized Scientific Research Platform that relied on Beijing Synchrotron Radiation Facility of the Chinese Academy of Sciences, Beijing Natural Science Foundation (2222087), Technology Innovation Program of Institute of High Energy Physics [Y9545130U2].

Appendix A. Supporting information

Supplementary data associated with this article can be found in the online version at doi:10.1016/j.nantod.2024.102626.

Data Availability

Data will be made available on request.

References

[1] L.R.H. Gerken, M.E. Gerdes, M. Pruschy, I.K. Herrmann, Mater. Horiz. 10 (2023) 4059–4082, https://doi.org/10.1039/d3mh00265a.
[2] J. Xie, L. Gong, S. Zhu, Y. Yong, Z. Gu, Y. Zhao, Adv. Mater. 31 (2019) e1802244, https://doi.org/10.1002/adma.201802244.
[3] J.Da Silva, C. Bienassis, P. Schmitt, C. Berjaud, M. Guedj, S. Paris, J. Exp. Clin. Cancer Res. 43 (2024) 11, https://doi.org/10.1186/s13046-023-02938-0.
[4] S. Kotb, A. Detappe, F. Lux, F. Appaix, E.L. Barbier, V.L. Tran, M. Plissonneau, H. Gehan, F. Lefranc, C. Rodriguez-Lafrasse, C. Verry, R. Berbeco, O. Tillement, L. Sancey, Theranostics 6 (2016) 418–427, https://doi.org/10.7150/thno.14018.
[5] C.L. Smith, S.P. Best, F. Gagliardi, T. Tominaga, M. Geso, Radiat. Meas. 106 (2017) 352–356, https://doi.org/10.1016/j.radmeas.2017.01.019.
[6] A.F. Bagley, E.B. Ludmir, A. Maitra, B.D. Minsky, G. Li Smith, P. Das, A.C. Koong, E. B. Holliday, C.M. Taniguchi, M.H.G. Katz, E.P. Tamm, R.A. Wolff, M.J. Overman, S. Patel, M.P. Kim, C.D. Tzeng, N. Ikoma, M.S. Bhutani, E.J. Koay, Clin. Transl. Radiat. Oncol. 33 (2022) 66–69, https://doi.org/10.1016/j.ctro.2021.12.012.
[7] S. Bonvalot, C. Le Pechoux, T. De Baere, G. Kantor, X. Buy, E. Stoeckle, P. Terrier, P. Sargos, J.M. Coindre, N. Lassau, R.Ait Sarkouh, M. Dimitriu, E. Borghi, L. Levy, E. Deutsch, J.C. Soria, Clin. Cancer Res. 23 (2017) 908–917, https://doi.org/10.1158/1078-0432.CCR-16-1297.
[8] S. Bonvalot, P.L. Rutkowski, J. Thariat, S. Carrere, A. Ducassou, M.P. Sunyach, P. Agoston, A. Hong, A. Mervoyer, M. Rastrelli, V. Moreno, R.K. Li, B. Tiangco, A. C. Herraez, A. Gronchi, L. Mangel, T. Sy-Ortin, P. Hohenberger, T. de Baere, A. Le Cesne, S. Helfre, E. Saada-Bouzid, A. Borkowska, R. Anghel, A. Co, M. Gebhart, G. Kantor, A. Montero, H.H. Loong, R. Verges, L. Lapeire, S. Dema, G. Kacso, L. Austen, L. Moureau-Zabotto, V. Servois, E. Wardelmann, P. Terrier, A.J. Lazar, J. Bovee, C. Le Pechoux, Z. Papai, Lancet Oncol. 20 (2019) 1148–1159, https://doi.org/10.1016/S1470-2045(19)30326-2.
[9] S. Bonvalot, P.L. Rutkowski, J. Thariat, S. Carrere, A. Ducassou, M.P. Sunyach, P. Agoston, A.M. Hong, A. Mervoyer, M. Rastrelli, V. Moreno, R.K. Li, B.J. Tiangco, A.C. Herraez, A. Gronchi, T. Sy-Ortin, P. Hohenberger, T. de Baere, A.L. Cesne, S. Helfre, E. Saada-Bouzid, R.M. Anghel, G. Kantor, A. Montero, H.H. Loong, R. Verges, G. Kacso, L. Austen, V.F. Servois, E. Wardelmann, M. Dimitriu, P. Said, A.J. Lazar, J. Bovee, C.L. Pechoux, Z. Papai, Int J. Radiat. Oncol. Biol. Phys. 114 (2022) 422–432, https://doi.org/10.1016/j.ijrobp.2022.07.001.
[10] C.Le Tourneau, Z. Takacsi-Nagy, L. Finzi, X. Liem, V. Calugaru, V. Moreno, E. Calvo, S. Salas, B. Doger, A. Dubray-Vautrin, X. Mirabel, N. Badois, A. Chilles, N. Fakhry, S.W.H. Kam, L. Houdas, A. Debard, O.I. Vivar, L.A. Farber, M. Lesnik, Int. J. Radiat. Oncol. 117 (2023). S99-S99.
[11] S.S. Yom, Z. Takacsi-Nagy, X. Liem, S. Salas, A. Debard, L. Finzi, O.I. Vivar, L. A. Farber, M. Gogishvili, G. Kristesashvili, T. Makharadze, C. Hoffmann, C. Le Tourneau, Int. J. Radiat. Oncol. 114 (2022). E313-E313.
[12] F.A. Hussain, S.E. Janisse, M.C. Heffern, M. Kinyua, J.M. Velazquez, iScience 25 (2022) 104138, https://doi.org/10.1016/j.isci.2022.104138.
[13] M. Pei, Y. Zhu, S. Liu, H. Cui, Y. Li, Y. Yan, Y. Li, C. Wan, Q. Wan, Adv. Mater. 35 (2023) e2305609, https://doi.org/10.1002/adma.202305609.
[14] A. Sahraneshin, S. Asahina, T. Togashi, V. Singh, S. Takami, D. Hojo, T. Arita, K. Minami, T. Adschiri, Cryst. Growth Des. 12 (2012) 5219–5226, https://doi.org/10.1021/cg3005739.
[15] X. Chen, R. Kang, G. Kroemer, D. Tang, Nat. Rev. Clin. Oncol. 18 (2021) 280–296, https://doi.org/10.1038/s41571-020-00462-0.
[16] Z. Deng, M. Xi, C. Zhang, X. Wu, Q. Li, C. Wang, H. Fang, G. Sun, Y. Zhang, G. Yang, Z. Liu, ACS Nano 17 (2023) 4495–4506, https://doi.org/10.1021/acsnano.2c10352.
[17] Z. Du, X. Wang, X. Zhang, Z. Gu, X. Fu, S. Gan, T. Fu, S. Xie, W. Tan, Angew. Chem. Int. Ed. Engl. 62 (2023) e202302525, https://doi.org/10.1002/anie.202302525.

[18] W. Huang, S. Shi, H. Lv, Z. Ju, Q. Liu, T. Chen, Bioact. Mater. 27 (2023) 560–573, https://doi.org/10.1016/j.bioactmat.2023.04.010.
[19] M. Lyu, M. Luo, J. Li, O.U. Akakuru, X. Fan, Z. Cao, K. Fan, W. Jiang, Adv. Funct. Mater. 33 (2023) e2306930, https://doi.org/10.1002/adfm.202306930.
[20] J. Wang, Z. Li, Z. Wang, Y. Yu, D. Li, B. Li, J. Ding, Adv. Funct. Mater. 30 (2020) e1910676, https://doi.org/10.1002/adfm.201910676.
[21] Z. Wang, X. Ren, Y. Li, L. Qiu, D. Wang, A. Liu, H. Liang, L. Li, B. Yang, A. K. Whittaker, Z. Liu, S. Jin, Q. Lin, T. Wang, ACS Nano 18 (2024) 10288–10301, https://doi.org/10.1021/acsnano.4c01625.
[22] W. Zhen, R.R. Weichselbaum, W. Lin, Adv. Mater. 35 (2023) e2206370, https://doi.org/10.1002/adma.202206370.
[23] F. Hu, J. Huang, T. Bing, W. Mou, D. Li, H. Zhang, Y. Chen, Q. Jin, Y. Yu, Z. Yang, Adv. Sci. 11 (2024) e230988, https://doi.org/10.1002/advs.202309388.
[24] S. Lu, Y. Li, Y. Yu, Adv. Mater. 36 (2024) e2404971, https://doi.org/10.1002/adma.202404971.
[25] P. Zheng, C. Zhou, L. Lu, B. Liu, Y. Ding, J. Exp. Clin. Cancer Res. 41 (2022) 271, https://doi.org/10.1186/s13046-022-02485-0.
[26] P. Tsvetkov, S. Coy, B. Petrova, M. Dreishpoon, A. Verma, M. Abdusamad, J. Rossen, L. Joesch-Cohen, R. Humeidi, R.D. Spangler, J.K. Eaton, E. Frenkel, M. Kocak, S.M. Corsello, S. Lutsenko, N. Kanarek, S. Santagata, T.R. Golub, Science 375 (2022) 1254–1261, https://doi.org/10.1126/science.abf0529.
[27] R. Li, W. Zhao, Z. Han, N. Feng, T. Wu, H. Xiong, W. Jiang, Small 20 (2024) e2306263, https://doi.org/10.1002/smll.202306263.
[28] P. Pei, Y. Wang, W. Shen, Q. He, X. Han, C. Zhang, Y. Xie, G. Zhou, Y. Zhao, L. Hu, K. Yang, Aggregate (2024) e484, https://doi.org/10.1002/agt2.484.
[29] W. Shen, P. Pei, C. Zhang, J. Li, X. Han, T. Liu, X. Shi, Z. Su, G. Han, L. Hu, K. Yang, ACS Nano 17 (2023) 23998–24011, https://doi.org/10.1021/acsnano.3c08875.
[30] L. Chen, J. Min, F. Wang, Signal Transduct. Target Ther. 7 (2022) 378, https://doi.org/10.1038/s41392-022-01229-y.
[31] H. Zhou, D. Tang, Y. Yu, L. Zhang, B. Wang, J. Karges, H. Xiao, Nat. Commun. 14 (2023) 5350, https://doi.org/10.1038/s41467-023-40826-5.
[32] Y. Liao, D. Wang, S. Zhu, R. Zhou, F. Rahbarizadeh, Z. Gu, Nano Today 44 (2022) 101510, https://doi.org/10.1016/j.nantod.2022.101510.
[33] D. Wang, Y. Liao, H. Zeng, C. Gu, X. Wang, S. Zhu, X. Guo, J. Zhang, Z. Zheng, J. Yan, F. Zhang, L. Hou, Z. Gu, B. Sun, Adv. Mater. (2024) e2313991, https://doi.org/10.1002/adma.202313991.
[34] W. Xie, Z. Guo, L. Zhao, Y. Wei, Prog. Mater. Sci. 138 (2023) 101145, https://doi.org/10.1016/j.pmatsci.2023.101145.
[35] J. Zhou, Q. Yu, J. Song, S. Li, X.L. Li, B.K. Kang, H.Y. Chen, J.J. Xu, Angew. Chem. Int. Ed. Engl. 62 (2023) e202213922, https://doi.org/10.1002/anie.202213922.
[36] G. Zhang, T. Xiong, X. Pan, Y. Zhao, M. Yan, H. Zhang, B. Wu, K. Zhao, L. Mai, Nano Res. 12 (2019) 905–910, https://doi.org/10.1007/s12274-019-2321-z.
[37] R. Cai, H. Xiang, D. Yang, K.T. Lin, Y. Wu, R. Zhou, Z. Gu, L. Yan, Y. Zhao, W. Tan, J. Am. Chem. Soc. 143 (2021) 16113–16127, https://doi.org/10.1021/jacs.1c06652.
[38] C. Hu, Z. Jiang, Q. Wu, S. Cao, Q. Li, C. Chen, L. Yuan, Y. Wang, W. Yang, J. Yang, J. Peng, W. Shi, M. Zhai, M. Mostafavi, J. Ma, Nat. Commun. 14 (2023) 4767, https://doi.org/10.1038/s41467-023-40418-3.
[39] D. Wang, Y. Liao, H. Yan, S. Zhu, Y. Liu, J. Li, X. Wang, X. Guo, Z. Gu, B. Sun, ACS Nano 16 (2022) 21186–21198, https://doi.org/10.1021/acsnano.2c09169.
[40] S. Le Caër, Water 3 (2011) 235–253, https://doi.org/10.3390/w3010235.